A facile co-precipitation synthesis of heterostructured ZrO_2|ZnO nanoparticles as efficient photocatalysts for wastewater treatment

Alberto Quintana[†], Ainhoa Altube[‡], Eva García-Lecina[‡], Santiago Suriñach[†], Maria Dolors Baró[†], Jordi Sort[†,§], Eva Pellicer[†,] and Miguel Guerrero[†]*

[†] Departament de Física, Facultat de Ciències, Universitat Autònoma de Barcelona, E-08193 Bellaterra, Spain

[‡] Surface Engineering Area, IK4-CIDETEC, Paseo Miramón, 196, E-20014 San Sebastián, Spain

[§] Institució Catalana de Recerca i Estudis Avançats (ICREA), Pg. Lluís Companys 23, 08010 Barcelona, Spain

Keywords: ZnO, ZrO_2, Nanoparticles, Photocatalysis, Water Remediation

Abstract

ZrO_2 decorated ZnO (ZrO_2|ZnO) nanoparticles (NPs) have been synthesized by a facile co-precipitation method in the presence of cetyltrimethylammonium bromide (CTAB) surfactant. The ZrO_2 amount in the NPs has been varied from 1.0%, 2.0%, 4.9% and 9.3% by weight. The resulting NPs are heterostructured and consist of a crystalline ZnO core (wurtzite phase) surrounded by an amorphous ZrO_2 layer. X-ray diffraction analyses support this observation. The NPs show a narrow size distribution and are slightly elongated. Compared to pure ZnO NPs, the hybrid ZrO_2|ZnO ones show enhanced photocatalytic activity toward the degradation of Rhodamine B under UV-Vis light. Such enhancement has been partly attributed to the increased amount of oxygen vacancies when ZrO_2 is incorporated into the NPs, as shown by X-ray photoelectron spectroscopy analyses.

1. Introduction

Territorial conflicts, unsustainable economic development, and climate change limit the access to clean water sources up to 40% of world population.[1] According to the World Health Organization, 663 million people lacked drinking water sources in 2015.[2] However, the expansion of industrial activity demands more and more water. Only in the United States of America, 68 billion liters of water are employed per day by industry.[3] For this reason, efficient wastewater treatments are essential to convert polluted water into a re-usable effluent. One of the main drawbacks is the complex chemical composition of wastewaters. Oils, organic solvents, adhesives, heavy metals, and dyes are common constituents. A large number of them are highly toxic and potentially carcinogenic.[4]

Nowadays, several approaches in the wastewater treatment involve adsorption (i.e., active carbon), filtration, sedimentation or chlorination.[5] However, all these processes show several disadvantages; they are time-consuming, expensive and also generate toxic side-products.[1] One promising alternative is photocatalytic degradation, by which organic compounds are broken into harmless substances under mild conditions with the assistance of light. During the last years, great efforts have been devoted to investigate the performance of zinc oxide (ZnO) as a photocatalyst. [6-9] ZnO is an abundant semiconductor with a high exciton binding energy (~60 meV at room temperature) and a wide bandgap (~3.30 eV). It can crystallize either in the thermodynamically stable wurtzite structure or in the metastable zinc-blende and high-pressure rock-salt phases. The catalytic properties of ZnO have been tackled in several studies. Altough TiO_2 is proven to be the best photocatalyst for the removal of dyes in waste water, it has been

claimed that the separation of TiO_2 after photocatalytic experiments is very difficult due to its fine size.[10] Meanwhile, ZnO possesses a band gap comparable to that of TiO_2 and its removal has proven to be quite simple as it settles down at the bottom of the photocatalytic reaction vessel quickly. It has also been claimed that TiO_2 has better photochemical stability than ZnO in aqueous solution but the latter is photochemically more active.[11] In the wurtzite structure, ZnO possesses two polar faces ((0001)-Zn and (0001)-O)[12] which have a positive impact on the photocatalytic response.[13,14] Nevertheless, bare surface of wurtzite ZnO structures presents poor separation efficiency of photo-generated e^--h^+ pairs[15,16] and high photocorrosion.[16,17] The catalytic properties of ZnO can be enhanced by modifying the energy band gap,[18] improving the absorption sensitization[19] or scaling down the dimensions of the catalyst,[13,20,21] so as, for example, to increase the exposure of more reactive facets.[22] The formation of heterostructures consisting of ZnO and other transition metals or semiconductors[15,23] can also lead to an enhancement of the catalytic behavior. It has been shown that the electric field created between two metal oxides in intimate contact avoids the electron-hole recombination and also modifies the amount of oxygen vacancies or unsaturated cations, affecting the acid-base behavior of the metal oxide, and therefore, tuning the catalytic properties.[24]

Zirconium oxide (ZrO_2) is also a wide bandgap semiconductor (~5.00 eV) whose catalytic activity has been widely studied.[25,26] However, it also has some drawbacks such as low quantum yield and high recombination of photo-generated electron-hole pairs, which hinders its further use as a photocatalyst.[27] ZnO and ZrO_2 components have been co-synthetized to render hybrid materials suitable for various catalytic applications.[28] For example, Crisci et al.[29] successfully synthesized $Zn_xZr_yO_2$ catalysts which enabled the occurrence of consecutive reactions to obtain isobutene. Kennedy et

al.[30] prepared pure ZnO, ZrO_2 and their coupled oxides and studied their performance toward the degradation of 2,4-dichlorophenol. Even ternary Cu(O)|ZrO_2|ZnO catalysts have been employed in the hydrogenation of dimethyl 1,4-cyclohexane dicarboxylate,[31] the production of methanol[32] or hydrogen.[33] Therefore it is clear that the combination of ZnO and ZrO_2 can furnish a hybrid material with interesting (photo)catalytic properties.

In this study, we report a facile and environmentally friendly synthesis of zirconium oxide|zinc oxide (ZrO_2|ZnO) heterostructured nanoparticles (NPs) and the in-depth characterization of their properties. Structural analyses indicate that amorphous ZrO_2 clusters decorate the surface of crystalline ZnO NPs. We show that these heterostructures present enhanced photocatalytic activity in the degradation of Rhodamine B (RhB) under UV-Vis irradiation compared to their single counterparts, evidencing the synergistic effect between ZnO and ZrO_2 components.

2. Experimental Section

2.1. Synthesis of ZrO_2|ZnO NPs

All chemicals were of analytical grade and used without further purification. ZnO and ZrO_2|ZnO NPs with varying ZrO_2 wt.% content (1.0%, 2.0%, 4.9% and 9.3%) denoted as 1%ZrZnO, 2%ZrZnO, 4.9%ZrZnO and 9.3%ZrZnO, respectively, were synthesized by co-precipitation method.[34,35] Pure ZnO NPs were produced by first dissolving 0.5945 g of $Zn(Ac)_2 \cdot 2H_2O$ (Ac = acetate) and the same quantity of cetyltrimethylammonium bromide (CTAB) in 25 mL of ethanol at 65 ºC while stirring vigorously. Aside, 0.3 g of KOH were dissolved in 13 mL of ethanol and also heated to 65 ºC. Then, the KOH solution was added to the zinc acetate solution and refluxed for 3 h until a white precipitate was obtained. The ZrO_2|ZnO NPs were obtained by adding 1, 2, 5 and 10

wt.% of $ZrOCl_2 \cdot 8H_2O$, respectively, to the ZnO reaction vessel. For comparative purposes, pure ZrO_2 NPs were synthesized following the procedure earlier described for 9.3%ZrZnO sample without the addition of $Zn(Ac)_2 \cdot 2H_2O$ salt. All the samples were centrifuged in water twice at 6000 rpm for 5 min. The whitish precipitate was collected and let to dry overnight at room temperature.

2.2. Morphological and structural characterization

The morphology and structure of the NPs were examined by field emission scanning electron microscopy (FE-SEM) using a Zeiss MERLIN microscope operated at 3.0 kV and 100 pA and high-resolution transmission electron microscopy (HRTEM) on a JEOL-JEM 2011 apparatus operated at 200 kV. High angle annular dark field scanning transmission electron microscopy (HAADF-STEM) images and Energy-dispersive X-ray spectroscopy (EDX) line profile analyses were performed on a FEI Tecnai G2 F20 microscope operated at 200kV and equipped with an EDAX super ultra-thin window (SUTW) X-ray detector. For electron microscopy observations, the NPs were dispersed in ethanol and subjected to sonication for 5 min. Afterwards, one drop of the suspension was deposited onto a Si chip for SEM purposes, whereas 4 μL of the dispersion were placed on a carbon coated Cu grid for (HR)TEM and STEM analyses. The crystallographic structure of the samples was studied by selected area electron diffraction (SAED) at the TEM and powder X-ray diffraction (XRD). XRD patterns were recorded on a Philips X'Pert diffractometer using the Cu Kα radiation (40 kV and 30 mA) in the 25°–75° 2θ range. The structural parameters (crystallite size, microstrains and cell parameter) were evaluated by fitting the full XRD patterns using the "Materials Analysis Using Diffraction" (MAUD) Rietveld refinement software.[36] X-ray photoelectron spectroscopy (XPS) analyses were carried out on a PHI 5500 Multitechnique System spectrometer (from Physical Electronics), equipped with a

monochromatic X-ray source ($K_{\alpha}Al$ line with energy of 1486.6 eV and 350 W), placed perpendicular to the analyzer axis and calibrated using $3d_{5/2}$ line of Ag with a full width at half maximum (FWHM) of 0.8 eV. Charging effects were corrected by referencing the binding energies to that of the adventitious C1s line at 284.5 eV. All spectra were deconvoluted using Gaussian functions and assuming parabolic background. The chemical composition of the samples was analyzed by inductively coupled plasma optical emission spectroscopy (ICP-OES) using a Perkin-Elmer, model Optima 4300DV. Dry powders were digested in a solution consisting of 3.9 mL MQ-Water and 100 µL of diluted aqua regia (3 HCl : 1 HNO_3) stabilized with 10 µL of HF.

2.3. Evaluation of photocatalytic activity

The photocatalytic activity of pure ZnO, ZrO_2, and ZrO_2|ZnO NPs was evaluated by following the decolorization of a 9 ppm RhB aqueous solution (Acros Organics, 99%, without further treatment). Solutions were prepared by mixing 1 mL of catalyst dispersion (58 mg/mL) and 9 mL RhB (10 ppm) solution. In addition to this, in each experiment, a blank RhB solution (without catalyst) was used as a control and reference sample. The reaction cells were placed in a SwiftCure IB irradiation cabin equipped with a mercury lamp. Following the recommendations given by ISO 10678:2010 standard, suitable cut-off filters were used to limit the wavelength radiation and avoid direct photolysis of the dye. The average light intensity used was 220 W, and the wavelength ranged from 320 to 500 nm, thus covering part of the ultraviolet (UV) and visible (Vis) domains. The photocatalytic experiments were conducted under continuous magnetic stirring at room temperature. After the suspensions had been conditioned for 60 min in dark to reach adsorption−desorption equilibrium, the light was turned on to initiate the reaction. Experiments were then conducted under UV-Vis irradiation for an overall time of 180 min. The pink color of the solutions faded

gradually with time as a consequence of the decomposition of RhB. Aliquots were withdrawn regularly (at 0, 15, 30, 60, 120, and 180 min) from the reaction vessel, and the NPs were removed with a centrifuge. The supernatant solutions were then placed in a UV-Vis spectrophotometer (Shimadzu UV-1603) to measure the absorption spectra of RhB (λ = 550 nm) as a function of irradiation time. The photocatalytic activity of the catalysts was calculated as C/C_0, where C_0 is the concentration of the test solution of RhB before irradiation and C is the concentration of RhB after UV-Vis irradiation. Optical diffuse reflectance spectra were measured at room temperature using the same UV-Vis instrument equipped with an integrating sphere attachment using NaF as a reference. In this case, KBr was used as supporting material.

3. Results and discussion

3.1. Structural and morphological characterization

XRD analyses were conducted to investigate the crystallographic structure of the ZrO_2|ZnO NPs (Figure 1a). Diffractions peaks were noted in all cases except for pure ZrO_2, all matching the wurtzite structure of ZnO (JCPDS 36-1451). No additional peaks attributed to either Zr or ZrO_2 were found, even for the highest amount of Zr (sample 9.3%ZrZnO). Pure ZrO_2 NPs were of amorphous nature, as indicated by the absence of reflections in its XRD pattern.[37] Furthermore, no shift of the diffraction peaks with Zr addition was observed (Figure 1b), hence ruling out the incorporation of Zr atoms into the ZnO crystal lattice.[16] Interestingly, a small hump gradually emerged in the 24-34º 2θ region upon increasing the Zr content (Figure 1b). For sample 9.3%ZrZnO, this hump perfectly overlaps that shown in the XRD pattern of pure ZrO_2. This indicates that ZrO_2|ZnO NPs are made of crystalline wurtzite ZnO and amorphous ZrO_2. The average crystallite size (<D>), microstrains ($<\varepsilon^2>^{1/2}$) and cell parameters (*a*, *c*) of the ZnO

wurtzite phase are listed in Table 1. The average crystallite size of ZnO slightly increases with the amount of Zr. Contrarily, the cell parameters *a* and *c* remain constant, being the values slightly higher than the tabulated ones.[38]

FE-SEM analyses indicated that the NPs were rather uniform in size (Figure 2a and 2c) and exhibited a rounded morphology (Figure 2b and 2d), apparently irrespective of the Zr content. Complementary morphological and structural information was obtained by HRTEM. The corresponding images and their respective insets (Figure 3a and c) revealed the anisotropic shape of the NPs (i.e., they were not as spherical as suggested by SEM). The occurrence of lattice fringes (Figure 3, see insets) was attributed to the main ZnO phase. Interestingly, the presence of an amorphous thin shell around the crystalline core was clearly observed in the NPs corresponding to sample 9.3%ZrZnO (Figure 3c). The SAED patterns show spotty rings whose interplanar distances all match those of wurtzite ZnO, thus confirming the nanocrystalline nature of pure ZnO core and the occurrence of amorphous ZrO_2 shell in heterostructured ZrO_2|ZnO samples (Figure 3b and d, respectively).

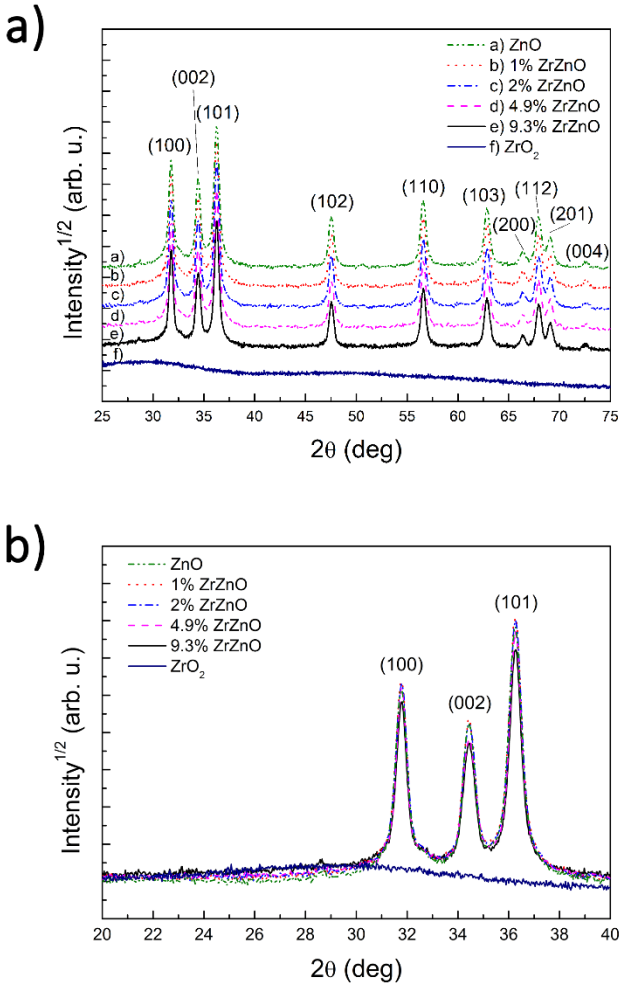

Figure 1. a) XRD patterns of pure ZnO, ZrO_2 and ZrO_2|ZnO NPs. b) Zoomed detail in the 2θ= 20°-40° region. Notice the hump gradually appearing in samples 1%ZrZnO-9.3%ZrZnO with increasing ZrO_2 content.

The particle size distributions for each sample were obtained by measuring 200 individual NPs from TEM images. The length and the width were taken into account separately (Supporting Information, Figure S1). The distributions were fitted to a log-normal function. Contrary to other metal-doped ZnO systems, the mean size of the NPs was kept fairly constant except for sample 9.3%ZrZnO (Supporting Information, Figure S2).[16,39] Moreover, the syntheses were proven to be highly reproducible since NPs

synthesized in different batches showed the same mean length and width (Supporting Information, Figure S3).

Table 1. Average crystallite size (<D>), microstrains ($<\varepsilon^2>^{1/2}$), and cell parameters (*a* and *c*) obtained through Rietveld refinement of the XRD patterns of pure ZnO and ZrO_2|ZnO NPs. According to JCPDS 36-1451, the theoretical cell parameters of wurtzite ZnO are *a* = 3.2498 Å and *c* = 5.2066 Å.

Sample		**ZnO**	**1%ZrZnO**	**2%ZrZnO**	**4.9%ZrZnO**	**9.3%ZrZnO**
<D> (nm)		31±2	33±4	34±4	35±2	37±4
$<\varepsilon^2>^{1/2} \cdot 10^{-4}$		12.4±0.4	14.8±0.1	15.4±0.3	16.6±0.4	14.3±0.2
Cell Parameters (Å)	***a***	3.253	3.254	3.254	3.255	3.254
	c	5.213	5.212	5.212	5.213	5.213

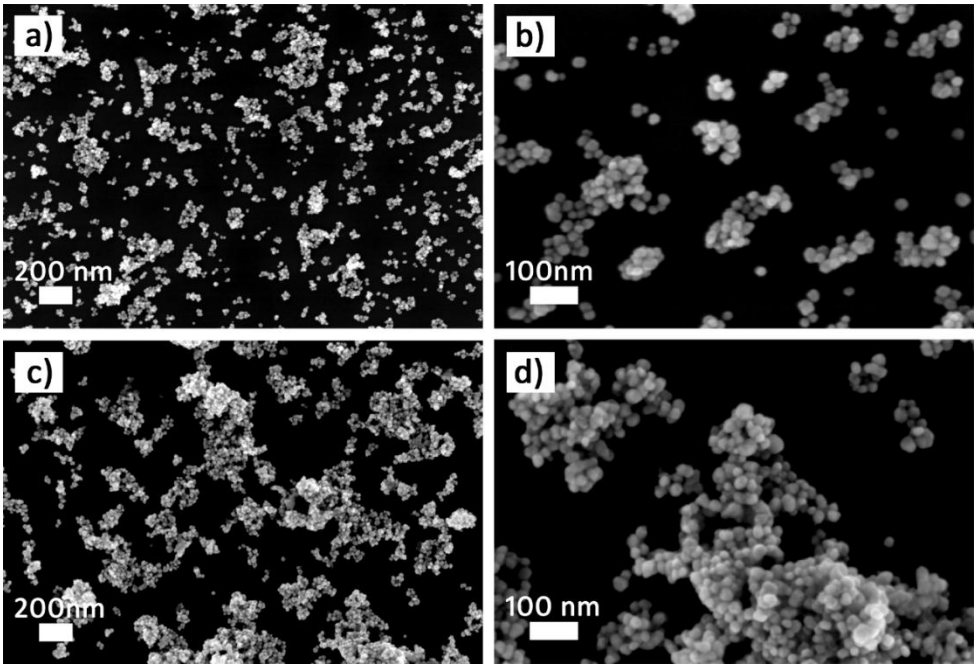

Figure 2. FE-SEM images of ZnO (a and b) and 9.3%ZrZnO (c and d) NPs.

It is believed that both the CTAB and the amorphous shell surrounding the ZnO cores modulate the NP size to some extent, mainly inhibiting their growth. In order to prove

whether CTAB had a noticeable effect on NP size, a new batch of NPs was produced through CTAB-free synthesis (see Supporting Information S4 for the size distributions). The length and width of the NPs synthesized with and without CTAB are listed in Table 2 for the sake of comparison. In the case of NPs obtained in CTAB-free syntheses, their length gradually decreases as the amount of ZrO_2 increases (from 1%ZrZnO to 9.3%ZrZnO). Meanwhile, their width remains fairly constant. Therefore, the presence of ZrO_2 in the NPs makes them more rounded. When the surfactant is added to the synthesis the length and the width of the NPs do not appreciably increase (or decrease) except for the highest Zr amount (9.3%ZrZnO). In this case, the size of the NPs synthesized with and without CTAB is virtually the same. This result indicates that CTAB effectively reduces the size of the NPs,[40] mainly their length, for low Zr contents. At higher ZrO_2 amounts such effect is less pronounced and even nonexistent.

Table 2. Average NP size (length and width, in nm) for samples 1%ZrZnO - 9.3%ZrZnO produced with and without CTAB.

Sample	With CTAB		Without CTAB	
	Length	**Width**	**Length**	**Width**
ZnO	22	16	35	18
1%ZrZnO	24	16	31	18
2%ZrZnO	22	15	27	17
4.9%ZrZnO	22	16	26	19
9.3%ZrZnO	26	18	26	19

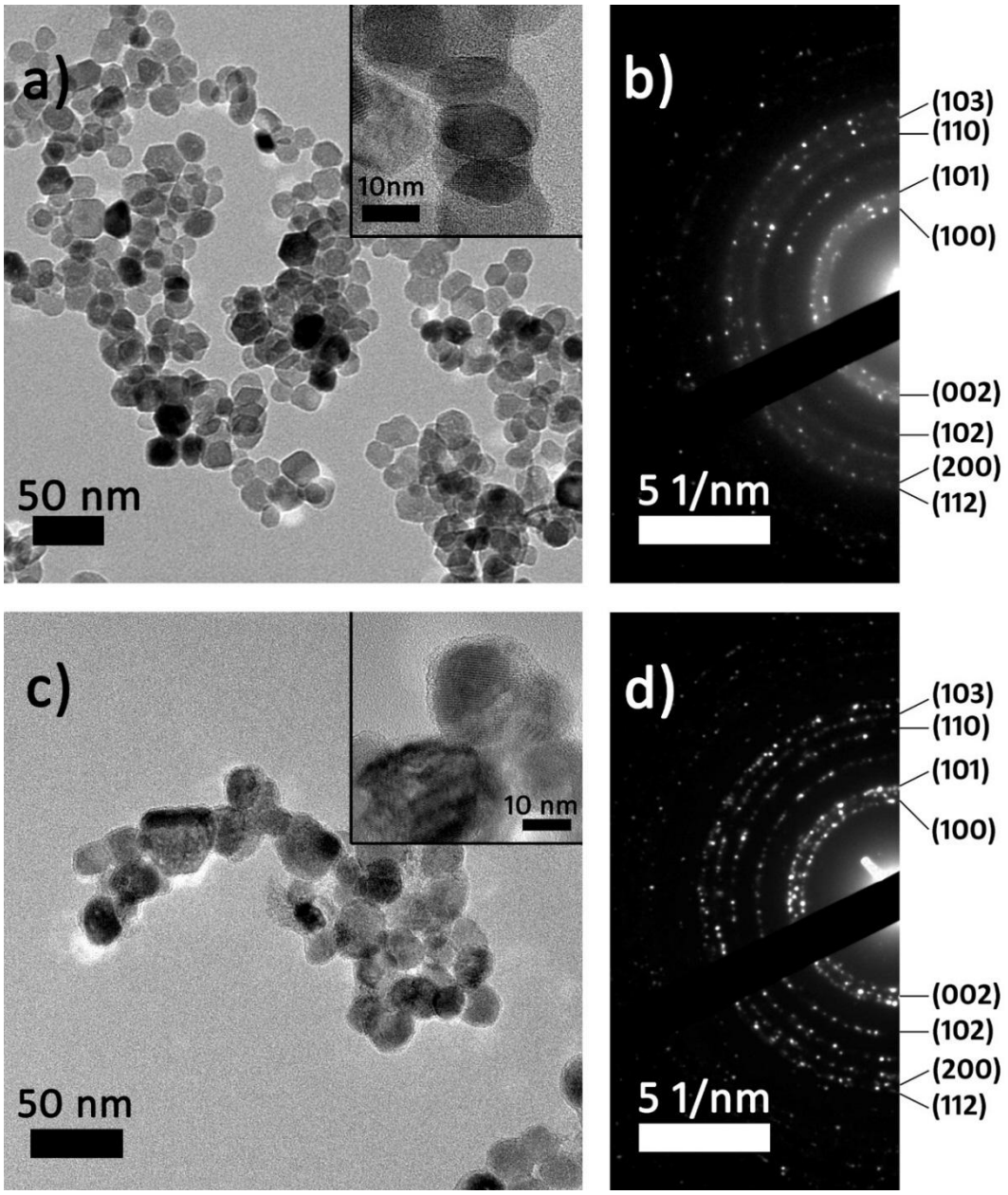

Figure 3. TEM and HRTEM images (insets) of a) pure ZnO and c) 9.3 wt.% ZrO_2 (9.3%ZrZnO) samples. The corresponding SAED patterns are shown in b) and d), respectively. The indexed planes correspond to wurtzite ZnO phase.

STEM-EDX analyses were conducted in order to shed light on the distribution of ZrO_2 component. As aforementioned, HRTEM analyses suggested the occurrence of an amorphous nanometer-thick layer coating the ZnO NPs (inset of Figure 3c). Indeed, STEM images showed the presence of groups of small entities surrounding the ZnO cores (Figure 4a). EDX line scan analysis performed across individual NPs indicated

that such entities are rich in Zr while the cores contain Zn (Figure 4b and c). Moreover, Zr was homogenously detected in all places of the sample (Supporting Information, Figure S5). Therefore, the resulting heterostructures can be described as crystalline ZnO cores coated by amorphous ZrO_2 clusters. In order to determine the actual amount of Zr in the NPs, they were digested for ICP-OES measurements. Table 3 lists the wt.% of ZrO_2 calculated from the Zr amounts measured. The results indicate that there is no significant difference between the nominal and the actual ZrO_2 amounts.

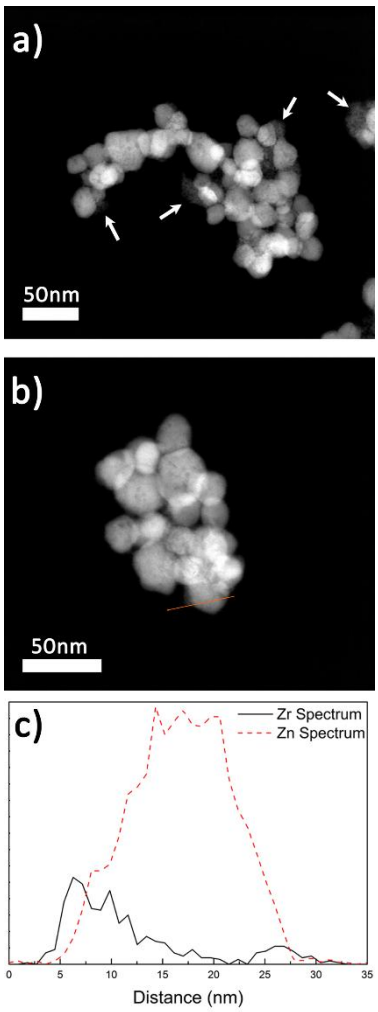

Figure 4. (a, b) HAADF-STEM images of sample 9.3%ZrZnO. Arrows in a) point to ZrO_2 clusters decorating the ZnO cores. c) EDX line spectra (Zr and Zn signals) taken across the red line in b). Zr is clearly detected at the shadow-like region visible on the left side of the NP.

Table 3. Theoretical and experimental ZrO_2 content (wt.%) in ZrO_2|ZnO NPs.

Sample	ZrO_2 content (wt.%)	
	Theoretical	Experimental
1%ZrZnO	1.0	1.1
2%ZrZnO	2.0	2.4
4.9%ZrZnO	4.9	5.5
9.3%ZrZnO	9.3	10.5

The oxidation states of Zn and Zr in ZnO and ZrO_2|ZnO NPs were investigated by means of XPS. Figure S6a and b shows the core-level spectra of Zn 2p transition (only $2p_{3/2}$) for samples ZnO and 9.3%ZrZnO, respectively. The corresponding O 1s transitions are shown in Figure 5a and 5b. Figure S6 depicts the Zr 3d transition for sample 9.3%ZrZnO. The Zn $2p_{3/2}$ spectra (Figure S6a and b) can be described as the superposition of two bands, a prominent one matching Zn^{2+} transition (1021.4 eV) and a weaker band at 1023.1eV attributable to $Zn(OH)_2$. The O 1s spectra (Figure 5a and b) can be deconvoluted into three peaks. The most intense band (~530.0 eV) corresponds to lattice oxygen[41] in ZnO (Figure 5a) and additionally in ZrO_2[42] (Figure 5b). The second peak (~531.5eV) can be attributed to carboxyl groups arising from unreacted acetate residues from the synthesis or, most likely, to oxygen vacancies.[43] Remarkably, the intensity of this band is slightly higher in the sample with ZrO_2 (9.3%ZrZnO, Figure 5b). For a more quantitative comparison, the intensity of the O 1s peaks has been normalized to the intensity of the lattice oxygen peak[44] in Table 4. It can be seen that the normalized intensity ratio of the peak attributed to either carboxyl groups or oxygen vacancies is higher in sample 9.3%ZrZnO. We speculate that this peak is mostly related to oxygen vacancies rather than carboxylate residues. Both samples, ZnO and 9.3%ZrZnO, were synthesized using the same amount of Zn acetate precursor, and hence, the contribution from carboxylate residues should be, a priori, the same.

Altogether, this indicates the formation of a large amount of oxygen vacancies during the synthesis.

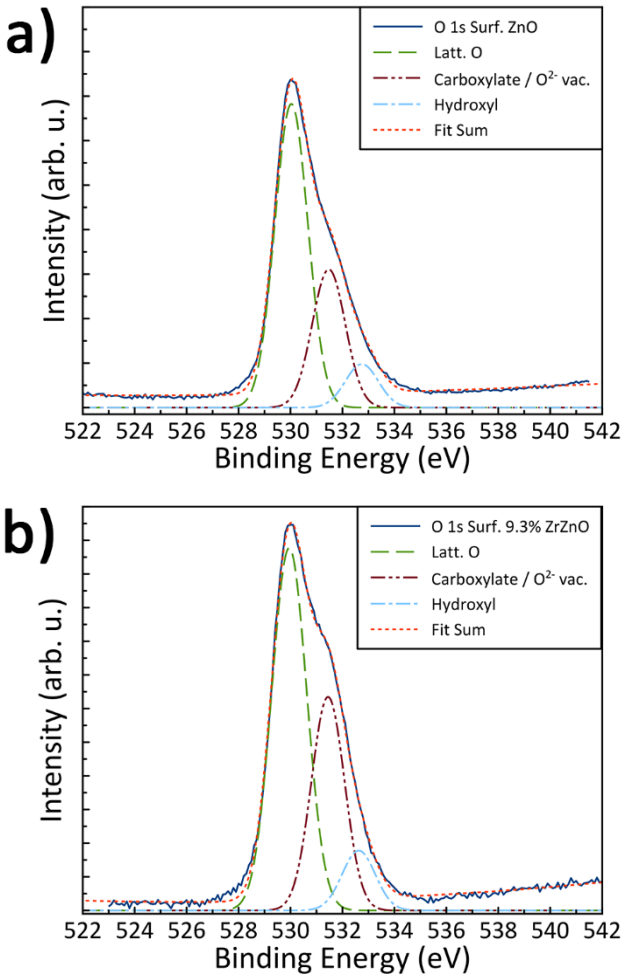

Figure 5. Core-level XPS spectra corresponding to the O 1s spectra of samples (a) ZnO and (b) 9.3%ZrZnO.

Table 4. Normalized peak intensity for the contributions to the core-level O 1s XPS spectra for ZnO and 9.3%ZrZnO NPs.

Energy (eV)		**ZnO**	**9.3%ZrZnO**
		O 1s (Surf)	**O 1s (Surf)**
Structural O	**530.0**	1	1
Carboxylate/O^{2-} vac.	**531.5**	0.46	0.59
Hydroxyl groups	**532.5**	0.14	0.17

The peak centered at 532.5eV is attributed to hydroxyl groups. Some authors have indeed reported the formation of a $Zn(OH)_2$ passive layer in ZnO NPs in contact with air.[34] Finally, the Zr 3d spectra (Figure S7) shows a doublet located at 182.0 and 184.2 eV, which match the binding energies expected for $3d_{3/2}$ and $3d_{5/2}$, respectively, of Zr^{4+}.[45]

3.2. Photocatalytic behavior

The photocatalytic behavior of the synthesized ZrO_2|ZnO NPs samples was evaluated by following the degradation of RhB under UV-Vis for 3 h soon after the adsorption-desorption equilibrium was reached. Figure 6a presents the C/C_0 ratio as a function of time, where C_0 is the initial concentration and C is the concentration at a given time of RhB.

A decrease is observed in the organic dye concentration when catalysts are present in the aqueous solution, the rate being faster and the concentration of degraded RhB higher when the amount of zirconia in the NPs is increased. To discard other possible contributions to the catalytic response, additional experiments were performed to ensure that light irradiation and ZrO_2 alone had little effect on RhB degradation. The results of both experiments are also shown in Figure 6a. As can be observed, no degradation occurred in the absence of ZnO (pure ZrO_2).

There are various factors associated to the photocatalytic activity of metal oxide-based NPs such as the morphology and the NP size.[46,47] As the NPs size is almost constant within sample series, or even slightly higher for the sample with the highest ZrO_2 amount (9.3%ZrZnO), the enhanced catalytic behavior cannot be attributed to an increase in the active surface area. Moreover, it was qualitatively observed by TEM that

the level of aggregation (and hence, interparticle porosity) was very similar among the different samples. Since the photocatalytic activity is also closely related to the light absorption capacity of the photocatalysts,[48] the UV-Vis diffuse reflectance spectra of all samples were measured and converted to the visualized absorption spectra (Figure 6b). The absorption spectra show stepped curves with a similar cut-off wavelength value around 390 nm irrespective of the photocatalyst. This value is in agreement with the corresponding bibliographic data.[49] Therefore, the enhancement in the catalytic behavior with the ZrO_2 content can be attributed neither to differences in their light absorption capacity. On the other hand, as expected, ZrO_2 shows no absorption at the wavelength range studied. Actually, the lack of activity of amorphous ZrO_2 is due to its large bandgap.[50]

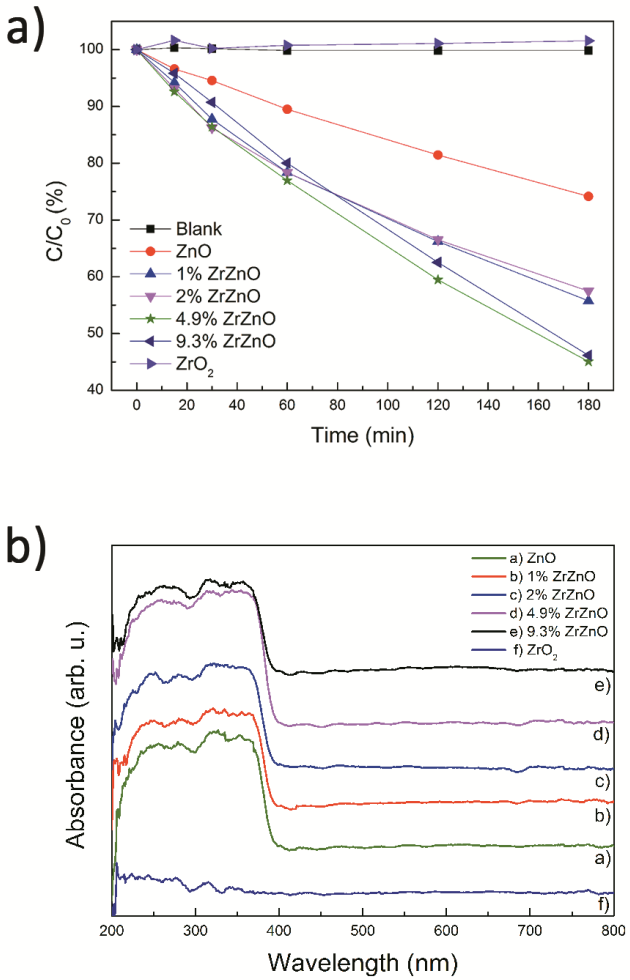

Figure 6. a) C/C_0 vs time plot showing the decrease of the dye concentration with time and b) UV-Vis absorption spectra for the different photocatalysts.

According to the literature, when ZnO NPs are irradiated, electrons are transferred from the valence band to the conduction band. Electron-hole pairs are then created on ZnO, which enable the photocatalytic process.[51] Surface defects are needed to separate and stabilize those photo-generated electron-hole pairs against their recombination. XPS measurements showed that the amount of defects (i.e., oxygen vacancies) indeed increases with Zr content. This could explain why the photocatalytic performance gradually improves from ZnO to 4.9%ZrZnO. However, a further increase in Zr concentration (from 4.9%ZrZnO to 9.3%ZrZnO) does not bring a further enhancement

of the photocatalytic activity. It is conjectured that an excessive amount of ZrO_2 increases the electron-hole pair recombination rate, thus inhibiting the photodegradation reaction.[52] Moreover, the active ZnO sites might become less accessible due to the ZrO_2 coating.

4. Conclusions

Heterostructured ZrO_2|ZnO NPs consisting of amorphous ZrO_2 clusters decorating crystalline ZnO cores have been obtained by a simple co-precipitation method in KOH. The formation of amorphous ZnO was evidenced by both XRD, HAADF-STEM and HRTEM analyses. Except for the sample with the highest ZrO_2 amount, both the length and the size of the NPs hardly varied with the ZrO_2 content. The hybrid samples outperformed both pure ZnO and ZrO_2 NPs in terms of photocatalytic behavior. The decolorization of RhB dye was faster when using ZrO_2|ZnO NPs as photocatalysts, being 4.9 wt.% ZrO_2 the optimum amount. An increased amount of surface defects like oxygen vacancies, as indicated by XPS, seem to be behind the enhanced photocatalytic response. Considering the simplicity of the fabrication process, we expect that these NPs could find uses in sustainable water remediation processes in the near future.

- **Author Information**

Corresponding Author e-mail: Eva.Pellicer@uab.cat

- **Acknowledgment**

Financial support by the Spanish Government (Projects MAT2014-57960- C3-2-R and MAT2014-57960- C3-1-R with associated FEDER), Generalitat de Catalunya (2014-SGR- 1015) and Basque Government (ELKARTEK, FN KK-2015/00101) is acknowledged. E.P. is grateful to MINECO for the “Ramon y Cajal” contract (RYC-2012-10839).

- **References**

[1] Pera-Titus, M.; García-Molina, V.; Baños, M. A.; Giménez, J; Esplugas, S. Degradation of Chlorophenols by Means of Advanced Oxidation Processes: A General Review. *Appl. Catal., B* **2004**, *47*, 219–256.

[2] Grojec, A. Progress on sanitation and drinking water – 2015 update and MDG assessment, *WHO Library Cataloguing-in-Publication Data*, **2015**.

[3] Kenny, J.F.; Barber, N.L.; Hutson, S.S.; Linsey, K.S.; Lovelace, J.K.; Maupin, M.A. Estimated use of water in the United States in 2005. U.S. Geological Survey Circular **2009**, *1344*, 1-52.

[4] Crini, G. Non-Conventional Low-Cost Adsorbents for Dye Removal: A Review. *Bioresour. Technol.* **2003**, *97*, 1061-1085.

[5] Mushtaq, F.; Guerrero, M.; Sakar, M. S.; Hoop, M.; Lindo, A. M.; Sort, J.; Chen, X.; Nelson, B. J.; Pellicer, E.; Pané, S. Magnetically Driven Bi_2O_3/BiOCl-Based Hybrid Microrobots for Photocatalytic Water Remediation. *J. Mater. Chem. A* **2015**, *3*, 23670-23675.

[6] Zhu, C.; Lu, B.; Su, Q.; Xie, E.; Lan, W. A Simple Method for the Preparation of Hollow ZnO Nanospheres for Use as a High Performance Photocatalyst. *Nanoscale* **2012**, *4*, 3060-3064.

[7] Lee, K. M.; Lai, C. W.; Ngai, K. S.; Juan, J. C. Recent Developments of Zinc Oxide Based Photocatalyst in Water Treatment Technology: A Review. *Water Res.* **2016,** *88*, 428-448.

[8] Tian, C.; Zhang, Q.; Wu, A.; Jiang, M.; Liang, Z.; Jiang, B.; Fu, H. Cost-Effective Large-Scale Synthesis of ZnO Photocatalyst with Excellent Performance for Dye Photodegradation. *Chem. Commun.* **2012**, *48*, 2858-2860.

[9] Chen, X.; Wu, Z.; Liu, D.; Gao, Z. Preparation of ZnO Photocatalyst for the Efficient and Rapid Photocatalytic Degradation of Azo Dyes. *Nanoscale Res. Lett.* **2017**, *12*, 143.

[10] Sangari, N. U.; Velusamy, P. Photocatalytic Decoloration Efficiencies of ZnO and TiO_2: A Comparative Study. *J. Env. Sci. Pollut. Res*. **2016**, 2, 42–45.

[11] Mondal, K.; Sharma A. Photocatalytic Oxidation of Pollutant Dyes in Wastewater by TiO_2 and ZnO nano-materials–A Mini-review. In: Nanoscience & Technology for Mankind **2014**, Chapter 5, The National Academy of Sciences India (NASI), Editors: Ashok Misra, Jayesh R. Bellare, pp. 36-72.

[12] Özgür, Ü.; Alivov, Y. I., Liu, C.; Teke, A.; Reshchikov, M. A.; Doğan, S.; Avrutin, V.; Cho, S.-J.; Morkoç, H. A Comprehensive Review of ZnO Materials and Devices. *J. Appl. Phys.* **2005**, *98*, 041301-1-01103-103.

[13] Huang, M.; Yan, Y.; Feng, W.; Weng, S.; Zheng, Z.; Fu, X.; Liu, P. Controllable Tuning Various Ratios of ZnO Polar Facets by Crystal Seed-Assisted Growth and their Photocatalytic Activity. *Cryst. Growth Des.* **2014**, *14*, 2179-2186.

[14] Jang, E. S.; Won, J.-H.; Hwang, S.-J.; Choy, J.-H. Fine Tuning of the Face Orientation of ZnO Crystals to Optimize their Photocatalytic Activity. *Adv. Mater.* **2006**, *18*, 3309-3312.

[15] Yan, F.; Wang, Y.; Zhang, J.; Lin, Z.; Zheng, J.; Huang, F. Schottky or Ohmic Metal-Semiconductor Contact: Influence on Photocatalytic Efficiency of Ag/ZnO and Pt/ZnO Model Systems. *ChemSusChem* **2014**, *7*, 101-104.

[16] Subash, B.; Krishnakumar, B.; Swaminathan, M.; Shanthi, M. Highly Efficient, Solar Active, and Reusable Photocatalyst: Zr-Loaded Ag-ZnO for Reactive Red 120 Dye Degradation with Synergistic Effect and Dye-Sensitized Mechanism *Langmuir* **2013**, *29*, 939-949.

[17] Weng, B.; Yang, M.-Q.; Zhang, N.; Xu, Y.-J. Towards the Enhanced Photoactivity and Photostability of ZnO Nanospheres via Intimate Surface Coating with Reduced Graphene Oxide *J. Mater. Chem. A* **2014**, *2*, 9380-9389.

[18] Das, S. C.; Green, R. J.; Podder, J.; Regier, T. Z.; Chang, G. S.; Moewes, A. Band Gap Tuning in ZnO Through Ni Doping Via Spray Pyrolysis *J. Phys. Chem. C* **2013**, *117*, 12745-12753.

[19] Yi, S.; Cui, J.; Li, S.; Zhang, L.; Wang, D.; Lin, Y. Enhanced Visible-Light Photocatalytic Activity of Fe/ZnO for Rhodamine B Degradation and its Photogenerated Charge Transfer Properties. *Appl. Surf. Sci.* **2014**, *319*, 230-236.

[20] Kim, S.; Kim, M.; Kim, T; Baik, H.; Lee, K. Evolution of Space-Efficient and Facet-Specific ZnO 3-D Nanostructures and their Application in Photocatalysis, *CrystEngComm* **2013**, *15*, 2601-2607.

[21] Al-Sabahi, J.; Bora,T.; Al-Abri, M.; Dutta, J. Controlled Defects of Zinc Oxide Nanorods for Efficient Visible Light Photocatalytic Degradation of Phenol. *Materials* **2016**, *9*, 238.

[22] Cho, S.; Jang, J.-W.; Lee, J. S.; Lee, K.-H. Exposed Crystal Face Controlled Synthesis of 3D ZnO Superstructures. *Langmuir*, **2010**, *26*, 14255-14262.

[23] Wang, Y.; Wang, Q.; Zhan, X.; Wang, F.; Safdar, M.; He, J. Visible Light Driven Type II Heterostructures and their Enhanced Photocatalysis Properties. *Nanoscale* **2013**, *5*, 8326 - 8339.

[24] Pham, T. N.; Sooknoi, T.; Crossley, S. P.; Resasco, D. E. Ketonization of Carboxylic Acids: Mechanisms, Catalysts, and Implications for Biomass Conversion *ACS Catal.* **2013**, *3*, 2456-2473.

[25] Bansal, P.; Chaudhary, G. R.; Mehta, S. K. Comparative Study of Catalytic Activity of ZrO_2 Nanoparticles for Sonocatalytic and Photocatalytic Degradation of Cationic and Anionic Dyes. *Chem. Eng. J.* **2015**, *280*, 475-485.

[26] Ciesielczyk, F.; Szczekocka, W.; Siwińska-Stefańska, K.; Piasecki, A.; Paukszta, D.; Jesionowski, T. Evaluation of the Photocatalytic Ability of a Sol-Gel-derived MgO-ZrO_2 Oxide Material. *Open Chem.* **2017**, *15*, 7-18.

[27] Vignesh, K.; Suganthi, A.; Min, B.-K.; Kang, M. Fabrication of Meso-Porous BiOI Sensitized Zirconia Nanoparticles with Enhanced Photocatalytic Activity Under Simulated Solar Light Irradiation. *Appl. Surf. Sci.* **2015**, *324*, 652-661.

[28] Ibrahim, M. M. Photocatalytic Activity of Nanostructured ZnO-ZrO_2 Binary Oxide Using Fluorometric Method. *Spectrochim. Acta Mol. Biomol. Spectrosc.* **2015**, *145*, 487-492.

[29] Crisci, A. J.; Dou, H.; Prasomsri, T.; Román-Leshkov, Y. Cascade Reactions for the Continuous and Selective Production of Isobutene from Bioderived Acetic Acid Over Zinc-Zirconia Catalysts. *ACS Catal.* **2014**, *4*, 4196-4200.

[30] Sherly, E. D.; Vijaya, J. J.; Selvam, N. C. S.; Kennedy, L. J. Microwave Assisted Combustion Synthesis of Coupled ZnO-ZrO_2 Nanoparticles and their Role in the Photocatalytic Degradation of 2,4-dichlorophenol. *Ceram. Int.* **2014**, *40*, 5681-5691.

[31] Zhang, S.; Hu, Q.; Fan, G.; Li, F. The Relationship Between the Structure and Catalytic Performance Cu/ZnO/ZrO_2 Catalysts for Hydrogenation of dimethyl 1,4-cyclohexane dicarboxylate. *Catal. Commun.* **2013**, *39*, 96-101.

[32] Huang, C.; Chen, S.; Fei, X.; Liu, D.; Zhang, Y. Catalytic Hydrogenation of CO_2 to Methanol: Study of Synergistic Effect on Adsorption Properties of CO_2 and H_2 in CuO/ZnO/ZrO_2 System. *Catalysts* **2015**, *5*, 1846-1861.

[33] Matsumura, Y.; Ishibe, H. High Temperature Steam Reforming of Methanol Over Cu/ZnO/ZrO_2 Catalysts. *Appl. Catal. B* **2009**, *91*, 524-532.

[34] Bian, S.-W.; Mudunkotuwa, I. A.; Rupasinghe, T.; Grassian, V. H. Aggregation and Dissolution of 4 nm ZnO Nanoparticles in Aqueous Environments: Influence of pH, Ionic Strength, Size and Adsorption of Humic Acid. *Langmuir* **2011**, *27*, 6059-6068.

[35] Beek, W. J. E.; Wienk, M. M.; Kemerink, M.; Yang, X.; Janssen, R. A. J. Hybrid Zinc Oxide Conjugated Polymer Bulk Heterojunction Solar Cells. *J. Phys. Chem. B* **2005**, *109*, 9505–9516.

[36] Young, R. A. *The Rietveld Method*; International Union of Crystallography, Oxford University Press: Oxford, 1995.

[37] Wan, C.; Lu, Y.; Sun, Q.; Li, J. Hydrothermal Synthesis of Zirconium Dioxide Coating on the Surface of Wood with Improved UV Resistance. *Appl. Surf. Sci.* **2014**, *321*, 38-42.

[38] Sundaresan, A.; Bhargavi, R.; Rangarajan, N.; Siddesh, U.; Rao, C. N. R. Ferromagnetism As a Universal Feature of Nanoparticles of the Otherwise Nonmagnetic Oxides. *Phys. Rev. B* **2006**, *74*, 161306-1-161306-4.

[39] Suwanboon, S.; Amornpitoksuk, P.; Sukolrat, A.; Muensit, N. Optical and Photocatalytic Properties of La-Doped ZnO Nanoparticles Prepared Via Precipitation and Mechanical Milling Method. *Ceram. Int.* **2013**, *39*, 2811–2819.

[40] Raja, K.; Ramesh, P. S.; Geetha, D.; Kokila, T.; Sathiyapriya, R. Synthesis of Structural and Optical Characterization of Surfactant Capped ZnO Nanocrystalline. *Spectrochim. Acta, Part A* **2015**, *136*, 155-161.

[41] Wang, J.; Wang, Z.; Huang, B.; Ma, Y.; Liu, Y.; Qin, X.; Zhang, X.; Dai, Y. Oxygen Vacancies Induced Band-Gap Narrowing and Enhanced Visible Light Photocatalytic Activity of ZnO. *ACS Appl. Mater. Interfaces* **2012**, *4*, 4024-4030.

[42] Filho, U. P. R.; Gushikem, Y.; Fujiwara; F. Y. Zirconium Dioxide Supported on α-Cellulose: Synthesis and Characterization. *Langmuir* **1994**, *10*, 4357–4360.

[43] Wu, J. M.; Chen, Y.-R.; Kao, W. T. Ultrafine ZnO Nanoparticles/Nanowires Synthesized on a Flexible and Transparent Substrate: Formation, Water Molecules, and Surface Defect Effects. *ACS Appl. Mater. Interfaces*, **2014**, *6*, 487-494.

[44] Rahimnejad, S.; He, J. H.; Chen, W.; Wu, K.; Xu, G. Q. Tuning the Electronic and Structural Properties of WO_3 Nanocrystals by Varying Transition Metal Tungstate Precursors. *RSC Adv.* **2014**, *4*, 62423-62429.

[45] Samson, K.; Śliwa, M.; Socha, R. P.; Góra-Marek, K.; Mucha, D.; Rutkowska-Zbik, D.; Paul, J.-F.; Ruggiero-Mikołajczyk, M.; Grabowsky, R.; Słoczyński, J. Influence of ZrO_2 Structure and Copper Electronic State on Activity of Cu/ZrO_2 Catalysts in Methanol Synthesis from CO_2. *ACS Catal.* **2014**, *4*, 3730-3741.

[46] Zhai, B.; Huang, Y. M. A Review on Recent Progress in ZnO Based Photocatalysts. *Optoelectron. Mater.* **2016**, *1*, 22–36

[47] Siwińska-Stefańska, K.; Zdarta, J.; Paukszta, D.; Jesionowski, T. The Influence of Addition of a Catalyst and Chelating Agent on the Properties of Titanium Dioxide Synthesized via the Sol-gel Method. *J. Sol-Gel Sci. Technol.* **2015**, *75*, 264-278.

[48] Sharma, J.; Vashishtha, M.; Shah, D. O. Crystallite Size Dependence on Structural Parameters and Photocatalytic Activity of Microemulsion Mediated Synthesized ZnO Nanoparticles Annealed at Different Temperatures. *Global J. Sci. Frontier Res. B* **2011**, *14*, 19-32.

[49] Rahman, Q. I.; Ahmad, M.; Misra, S. K.; Lohani, M. Effective Photocatalytic Degradation of Rhodamine B Dye by ZnO Nanoparticles. *Mater. Lett.* **2013**, *91*, 170–174.

[50] El Hakam, S. A.; El-Dafrawy, S. M.; Fawzy, S.; Hassan, S. M. Structural, Photocatalytic and Antibacterial Activity of ZnO and ZrO_2 Doped ZnO Nanoparticles. *Int. J. Sci. Res.* **2014**, *3*, 779-787.

[51] Zhang, X.; Qin, J.; Xue, Y.; Yu, P.; Zhang, B.; Wang, L.; Liu, R. Effect of Aspect Ratio and Surface Defects on the Photocatalytic Activity of ZnO Nanorods. *Sci. Rep.* **2014**, *4*, 4596-1 – 4596-8.

[52] Selvam, N. C. S.; Vijaya, J. J.; Kennedy, L. J. Effects of Morphology and Zr Doping on Structural, Optical, and Photocatalytic Properties of ZnO Nanostructures. *Ind. Eng. Chem. Res.* **2012**, *51*, 16333-16345.